REVISION 2

Timescales of magma storage and migration recorded by olivine crystals in basalts of the March-April 2010 eruption at Eyjafjallajökull volcano, Iceland

Marco Viccaro*, Marisa Giuffrida, Eugenio Nicotra, Renato Cristofolini

Università di Catania, Dipartimento di Scienze Biologiche, Geologiche e Ambientali – Sezione di Scienze della Terra, Corso Italia 57, I-95129, Catania, Italy

*Corresponding Author: Marco Viccaro, Università di Catania, Dipartimento di Scienze Biologiche, Geologiche e Ambientali – Sezione di Scienze della Terra, Volcanology Research Group, Corso Italia 57, I-95129 Catania, Italy; telephone: +39 095 7195741; Fax: +39 095 7195760; e-mail: m.viccaro@unict.it; website: www.volcanology-unict.it

Abstract

The early eruptive phase of the 2010 eruption at the Fimmvörðuháls Pass, east of Eyjafjallajökull volcano, produced poorly evolved basalts with mildly alkaline affinity, and benmoreitic tephra were emitted during the second explosive phase from the summit vent of the volcano. In this study, textural features and chemical zoning preserved in olivine crystals of the early erupted basalts have been used in order to define the timescales of differentiation processes and magma ascent before the eruption. These lavas contain a mineral assemblage constituted by olivine (Fo_{70-88}) and plagioclase (An_{57-83}) in rather similar proportions with scarce clinopyroxene and opaque oxides. Olivine occurs as euhedral or embayed crystals characterized by different core compositions and zoning patterns. Three main olivine populations have been found, namely crystals with: a) wide Fo_{88} cores with normal zoning towards narrow rims (P1); b) ~Fo_{81} cores with either no zoning or slight reverse zoning patterns towards the rims (P2); c) ~Fo_{77} cores with reverse zoning at the rims (P3). The

olivine reverse zoning indicates that these poorly evolved magmas experienced mixing processes in addition to limited fractional crystallization at different levels of the plumbing system. Timescales of transfer dynamics before the eruption have been estimated through Fe-Mg diffusion modelling on these olivine populations. The olivine-melt equilibration through diffusion was triggered by interaction of magmas differing in their evolutionary degree. P1 and P2 crystals recorded a first event of interaction in a ~22-km-deep reservoir that took place about one month before the emission of the analysed products. Only part of P2 crystals records reverse zoning due to interaction with more basic magma bearing P1 crystals (which consequently develop normal zoning), suggesting fast timescales of magma mixing that prevented the complete homogenization. A second mixing event, that is evident in the P3 olivines, occurred at shallower levels (5-6 km of depth) ~15 days before the emplacement and can be considered the triggering mechanism leading to the eruption at the Fimmvörðuháls Pass. Integration of our timescales with seismic data relative to the hypocentre migration indicate rates of magma ascent throughout the deep plumbing system of ~0.01 m/sec. This study provides evidence that magmas emitted at Eyjafjallajökull volcano, and more in general at similar other volcanic systems in ocean ridge settings, can undergo complex processes during their storage and transport in the crust, chiefly due to the presence of a multi-level plumbing system.

Keywords: Eyjafjallajökull, olivine, diffusion modeling, magma mixing, ascent dynamics.

Introduction

Recent studies chiefly based on geophysical considerations have profoundly changed the view of a single-level, molten system of reservoirs distributed beneath the mid ocean ridges (e.g., Dunn et al., 2000, and references therein). Mush zones constituted of liquid regions of

variable dimensions and other portions characterized by various degrees of crystallization are thought more plausible to describe the physical configuration of magma storage zones beneath ocean ridges. The idea of a multi-level plumbing system, articulated through distinct paths of magma ascent, is more pronounced for important volcanic systems above ocean ridges characterized by central activity. The best examples of such kind are the Icelandic shield volcanoes (e.g., Katla, Eyjafjallajökull, Askja, Krafla, Grimsvötn, Bardarbunga). Magma transfer dynamics from the source zones up to the surface and eruption at these volcanic systems are not always easily understood, and requires that chemical and physical constraints are first made for the magma reservoirs (location, sizes, timescales of magmatic processes etc.).

The presence of zoning in crystals is evidence for changes of the chemical and/or physical conditions of the magmatic system such as melt composition, oxygen fugacity, temperature, pressure, volatile contents during their growth history (Wallace and Bergantz, 2002; 2004; 2005; Ginibre et al., 2007; Streck, 2008; Viccaro et al., 2010; Kahl et al., 2011; 2013). Furthermore, diffusion chronometry applied to compositionally zoned crystals has proved to be valuable for understanding either the reasons for or the timescales that lead to such changes (e.g. Zellmer et al., 1999; Costa et al., 2003; Costa and Chakraborty, 2004; Costa et al., 2008; Costa and Morgan, 2010; Morgan et al., 2004; Morgan and Blake, 2006; Kahl et al., 2011; 2013). As the crystals record physical and chemical changes of the magmatic environment, the intra-crystalline diffusion starts and the chemical gradient among different zones of the crystal is reduced over time. The extent to which the zoning will be equilibrated by diffusion depends on many parameters such as the mineral structure, the elements involved in the process, temperature and time. Thus, the zoning patterns preserved in minerals could be used to reconstruct the evolutionary processes that magmas underwent throughout the

plumbing system and the duration of storage and transport in different environments, which together are among the most important goals of the modern volcanology.

In this study, the textural features and chemical zoning preserved in olivine crystals have been used to track the pre-eruptive history of basaltic magmas feeding the early phase of the 2010 eruption of Eyjafjallajökull volcano at the Fimmvörðuháls Pass. Estimations on timescales of magmatic processes acting beneath the Eyjafjallajökull volcano have been obtained by modeling the Fe-Mg diffusion observed in olivine chemical profiles. Our results provide elements to understand the nature and timing of magmatic processes before the eruption of primitive basalts in Iceland that, although infrequent, can ~~have~~ present a significant hazard due to the limited timespan occurring between the beginning of magma ascent and the final magma extrusion.

The Eyjafjallajökull volcano

Geological setting and volcanism

Eyjafjallajökull volcano rises to a height of 1666 m at the southwestern end of the East Volcanic Zone (EVZ), which at present represents the most volcanically active region in Iceland (Fig. 1a). The EVZ is a propagating SW-NE trending rift located outside the main zone of spreading (the axial rift). This area includes 30 volcanic systems that, on the whole, account for ~79% of the total volume of erupted magmas in Iceland during the last 11 centuries. However, most of the emitted magma is accommodated by the active systems of Katla, Grimsvötn, Hekla and Bardarbunga-Veidivötn (Fig. 1a; Thordarson and Larsen, 2007). The EVZ is dominated by emission of tholeiitic magmas in its northeastern segment, whereas mildly alkaline magmas characterize the southwestern segment, which is currently propagating southwesterly (Thordarson and Larsen, 2007 and references therein).

Eyjafjallajökull has been constructed through sub-glacial eruptions and its edifice is completely covered by an ice cap. Historic activity of Eyjafjallajökull has been characterized by long-lasting periods of quiescence, commonly interrupted by initial hydromagmatic explosions evolving to eruptive episodes with Strombolian to sub-Plinian styles. Prior to the 2010 AD eruption, the historical record includes a radial fissure eruption dated ~920 AD and two small-volume summit eruptions at 1612 AD and 1821-1823 AD, which were identified through chrono-stratigraphic studies and analysis of historic chronicles (Thordarson and Larsen, 2007; Dugmore et al., 2013 and references therein). Extensive intrusions at 4.5 and 6.5 km of depth, with estimated volumes of 10-17×10^6 m^3 and 21-31×10^6 m^3 respectively, occurred beneath the Eyjafjallajökull volcano in 1994 and 1999, as revealed by InSAR observations, GPS geodetic measurements, and optical tilt leveling (Pedersen and Sigmundsson, 2004; 2006; Sturkell et al. 2003; Sigmundsson et al., 2010).

All the historic eruptions of Eyjafjallajökull were more or less contemporaneous with eruptions or evidence of magma movements [i.e., glacier floods and several small earthquakes] at the nearby Katla volcano (~25 km to the east). This trend held during the 2010 eruption at Eyjafjallajökull, as demonstrated by several seismic swarms beneath Katla in the 2011-2012 period. Sturkell et al. (2003) also argued that magma movements took place at shallow levels beneath Katla in 1999 at the same time of a magma intrusion beneath Eyjafjallajökull, both evidenced by GPS and seismic data.

The March-May 2010 eruption

The 2010 event at Eyjafjallajökull volcano was characterized by two distinct eruptive phases: an initial effusive flank eruption, characterized primarily by eruption of lava flows at the Fimmvörðuháls Pass (Fig. 1b), and a second explosive summit eruption producing ash-tephra fall-out that had heavy impact on air-traffic in a large part of Europe. Three months of

126 intense seismicity and deformation preceded the onset of the flank eruption on March 20,
127 2010 (Gudmundsson et al., 2010; Sigmundsson et al., 2010; Sigmarsson et al., 2011, and
128 references therein). Over the previous 18 years, several signals of volcanic unrest were
129 detected through geodetic and geophysical investigations, such as earthquakes and flank
130 deformation attributed to magma injections beneath the volcano. Precursory signals, recorded
131 since late December 2009, were the prelude of the opening on March 20, 2010 of a ~300 m
132 long fissure at Fimmvörðuháls Pass, between the Eyjafjallajökull and the Myrdalsjökull
133 glaciers (Figs. 1b and 2). The eruption produced lava fountains up to 150-m-high and limited
134 tephra fall-out. On March 31, a new fissure opened with an angle of 50° from that of March
135 20 (trending N15°W), where on April 2 the eruptive activity moved. The activity produced a
136 northward expanding small a'a lava flow field, filling deep gullies excavated on the flanks of
137 the Eyjafjallajökull volcano and forming spectacular lava falls (Fig. 2). Effusions from these
138 fissures continued until April 12, with an average magma emission rate of ~13 m^3/s
139 (Sigmundsson et al., 2010). This led to the formation of two small scoria cones at the active
140 vents and a lava field of basalts with mildly alkaline affinity (Sigmarsson et al., 2011; Keiding
141 and Sigmarsson, 2012; Moune et al., 2012). At the end of the flank eruption, the estimated
142 total volume of emitted magma was approximately 25×10^6 m^3 (Sigmundsson et al., 2010 and
143 references therein).

144 After just two days of rest, the volcanic activity started again in the early morning of April
145 14 at the central crater of Eyjafjallajökull volcano, preceded by a seismic swarm with
146 hypocentres fast moving from 7 km depth toward the ice-capped summit of the volcano
147 (Tarasewicz et al., 2012). The magma-ice interaction gave rise during the first days to a
148 hydromagmatic, highly explosive central eruption that produced a ~10 km-high ash plume
149 (Sigmundsson et al., 2010 and references therein; Sigmarsson et al., 2011). Thereafter, the
150 hydromagmatic activity decreased and evolved to purely magmatic after less than one week.

Main peaks of the explosive activity were recorded at the onset of the summit eruption and later on 5-6 May, with emission rates on the order of 10^6 kg/s (Sigmarsson et al., 2011). The sustained magma discharge continued until May 22 with emission of fine ash and dust with benmoreitic-trachytic composition.

Sampling and analytical methods

A total of 16 volcanic rock samples was collected from the last-emitted products of the lava flow field developed between March 20-April 12 2010 during the eruption at ~~the~~ Fimmvörðuháls Pass, east of the summit of Eyjafjallajökull volcano (Figs. 1b and 2). Samples are from the activity of April 10-12, just before the end of the eruption. Polished thin sections have been made for petrographic and textural analysis ~~on~~ of olivine crystals as well as for in situ microanalysis. High-contrast back-scattered electron (BSE) images, elemental x-ray maps and microanalytical data were obtained at the Dipartimento di Scienze Biologiche, Geologiche e Ambientali of Catania, Italy, on ~50 selected olivine crystals representative of the identified dimensional classes and textures ~~by~~ using a Tescan Vega-LMU scanning electron microscope equipped with an EDAX Neptune XM4-60 energy dispersive system, which is characterized by an ultra-thin Be window, coupled with an EDAX WDS LEXS (wavelength dispersive low energy x-ray spectrometer) calibrated for light elements. Operating conditions were set at 20 kV accelerating voltage and ~8 nA beam current for obtaining high-contrast BSE images. At the same operating conditions, elemental x-ray maps have been acquired with dwell time of 500 µs for 128 frames (total time for acquisition of each x-ray map around 4.5 hours). Operating conditions for the analysis of major element abundances in olivine and the other mineral phases were set at 20 kV accelerating voltage and 0.2 nA beam current. Repeated analyses on internationally certified Fo-rich olivine and glass

internal standards during the analytical runs ensure precision for all the collected elements on the order of 3-5% (all data available in the ESM 1).

Characteristics of the volcanic rocks

Petrography and chemistry of minerals

Volcanic products erupted during the first phase of the 2010 eruption at Eyjafjallajökull are basalts (Sigmarsson et al., 2011; Keiding and Sigmarsson, 2012; Moune et al., 2012) with rather homogeneous petrographic features. Differences are mainly related to groundmass textures and the modal abundance of mineral phases. Samples are mildly porphyritic (15 to 20 vol.% of phenocrysts) and highly vesiculated; phenocrysts mostly consist of plagioclase and olivine in similar proportions, together making up 80-85 vol.% of the total phenocryst content (Fig. 3a). The mineral assemblage also includes scarce clinopyroxene (~10-15 vol.%) and opaque oxides (<5 vol.%). Phenocrysts generally occur as single crystals with variable grain sizes. Glomerophyric structures involving olivine, plagioclase and clinopyroxene are also present. The groundmass is vitrophyric to hyalopilitic with plagioclase microlites as the predominant phase (Fig. 3a).

Plagioclase crystals vary in size from large crystals (up to 2400 μm) to micro-phenocrysts (~200 μm) with labradorite (An_{53}) to bytownite (An_{83}) compositions (Fig. 3a; Table ESM 1). The medium-size (500-1500 μm) plagioclase generally occurs as euhedral crystals, tabular in shape and rather homogeneous in composition. Analyses under the polarized light microscope do not reveal significant optical zoning. Also skeletal, swallow-tailed microlites are present in the analysed sections. The largest grains commonly exhibit a coarsely-sieved core, embedded by oscillatory-zoned outer rims. Phenocrysts affected by extensive dissolution (rounded edges) or with sieve-textures at the rim have been also found.

Olivines are present as large euhedral to anhedral phenocrysts up to ~4.5 mm in size (Fig. 3a-d). Most of the largest grains are strongly destabilized with extensive embayments that extend deeply into the crystal core; these embayments do not show reaction rims. Smaller crystals (from ~200 to 600 μm) are generally euhedral, though some of them have slight embayed morphology. Olivine core compositions vary from Fo_{88} to Fo_{77} (see Table ESM 1). In this regard, rim-to-rim major element profiles allowed three main crystal populations to be identified. Details of textural features and zoning patterns of the three populations are described in the following section.

Clinopyroxenes mostly occur as small euhedral phenocrysts ranging in size from 200 to 600 μm, rarely found as large single crystals (up to 1200 μm in size) or in aggregates with plagioclase and olivine. Their compositions are in the range Wo_{38-45}, $En_{40-51,}$ Fs_{12-16} (see Table ESM 1).

Two opaque oxides have been identified with compositions either of titaniferous-magnetite or Cr-spinel (Table ESM 1). The former is from subhedral to euhedral, with sizes up to few tens of μm, whereas the latter commonly occurs as anhedral crystals, up to 200 μm in size, enclosed in the largest olivine crystals with Fo_{88} and Fo_{81}.

Textural and compositional features of olivine crystals

Major element analyses were performed along rim-to-rim profiles on olivine crystals with sizes ranging from ~400 μm to 2500 μm. Traverses crosscut the centre of the crystal, with step of 7-13 μm between each analysed spot. Three main olivine populations have been identified on the basis on their core compositions, namely: 1) the first population (P1) refers to olivine with Fo_{88} cores (Fig. 3b); 2) the second population (P2) pertains to olivine with ~Fo_{81} cores (Fig. 3c); 3) the third population (P3) is constituted by olivine cores at ~Fo_{77} (Fig. 3d; Table ESM 1).

The P1 olivines (~Fo_{88}) are resorbed with extensive embayments (Fig. 4). They are rather uncommon (2-3 individuals per thin section) and typical of the largest phenocryst (900-2500 μm across). P1 olivines display nearly flat compositional profiles at their wide cores and normally zoned rims, decreasing to Fo_{70} at the outermost rim (50-80 μm).

Olivines belonging to P2 and P3 include euhedral or embayed large crystals with size ranging from 900 to 1500 μm or smaller olivines (~600 μm). P2 crystals constitute the most abundant population, being ~70% of the olivine phenocrysts observed in the analysed rocks (Fig. 5). These olivines show two distinct zoning patterns: a) rather constant ~Fo_{81} core composition and normally zoned rims, which is the dominant zoning pattern in P2; b) reverse zoning with slightly increasing Fo toward the rim (up to ~Fo_{83}), which occurs less commonly than normal zoning. Independently from the zoning pattern type, all the P2 crystals record a sudden drop to Fo_{73} in the outermost envelopes (last 30-50 μm).

All the P3 olivine crystals have core compositions at ~Fo_{77} with a marked reversely zoning toward the rims (Fig. 6). Variable ΔFo in the reverse zoned portion of crystals leads to define two sub-populations: P3a) with minor variations (~ΔFo_5), shifting the rim composition from ~Fo_{77} to ~Fo_{82}; P3b) with slightly more consistent changes (~ΔFo_8) that produce ~Fo_{85} envelopes. The outermost rims are normally zoned with decreasing Fo content to ~Fo_{70}.

Storage zones and processes

Compositional differences of the three populations of olivine crystals, which were found in the volcanic rocks emitted at the Fimmvörðuháls Pass during the 2010 eruption, necessarily imply the presence of three different magmatic environments characterised by changes of one or more of the above mentioned chemical-physical parameters. Various studies of Fe-Mg partitioning between olivine and basaltic liquids showed that the $^{Ol/Liq}K_{DFe\text{-}Mg}$ varies little with temperature and melt composition, being rather constant at 0.30 under pressures <2-3 GPa

(Roeder and Emslie, 1970). Conversely, the pressure dependence of $^{Ol/Liq}K_{DFe\text{-}Mg}$ is more marked, in a way that it is positively correlated with pressure (Herzberg and O'Hara, 1998; Putirka, 2005; Toplis, 2005). This means that olivines crystallizing from liquids rather similar in their temperature and composition evolve to lower Fo contents under decreasing pressure.

The physical and chemical conditions of crystallization for the three olivine populations have been constrained through two-step thermodynamic modelling using the MELTS code (Ghiorso and Sack, 1995; Asimow and Ghiorso, 1998). A mantle-equilibrated composition of the 2010 Eyjafjallajökull lavas has been chosen as the starting liquid and considered the parental liquid for all the three populations, even though we have evidence for open-system processes (i.e., magma mixing). However, mixing occurred between magmas similar in their compositions, which means that errors deriving from the use of a single, evolving composition through fractional crystallization modelled by MELTS are restricted. Effects due to the rather limited fractionation of these magmas have been removed by adding ~10-15% of Fo_{88} olivine until the calculated liquid has the crystallizing olivine with Fo_{88}, representative of equilibrium with a primary magma at mantle conditions (P1 olivines). In the first step of simulation, we have tried to reproduce the physical-chemical conditions of crystallization for the P2 olivines (~Fo_{81}) using the range of physical-chemical parameters defined through geothermobarometry by Keiding and Sigmarsson (2012) for the crystallization of these basalts, i.e.: pressure between 600 and 650 MPa, temperature between 1161°C and 1174°C, H_2O between 0.5 and 0.9 wt.%. For this reason, parameters have been set as follows for the first step of simulation: pressure between 630 and 600 MPa (representative of crystallization at 24-23 km of depth for a crust density of 2.8 g/cm^3; cf. Tarasewicz et al., 2012), temperature between 1180°C and 1160°C, H_2O = 0.7 wt.%. Several attempts (n >100) have been done, crossing the above-defined *X-P-T* parameters. However, P2 olivines (~Fo_{81}), coexisting with orthopyroxene and clinopyroxene of augitic composition, starts to crystallize at pressure of

615 MPa only if temperature is raised at 1210°C and fO_2 fixed at the NNO buffer (~3.5×10^{-3} Pa). Lower temperatures or more oxidizing redox conditions do not allow crystallization of P2 olivines and the associated paragenesis. Assuming that more fayalitic olivines (such as P3 olivines at ~Fo_{77}) are produced through crystallization from a slightly more evolved liquid and/or at different physical conditions, there is needing of a further simulation at changed chemical-physical conditions. The final liquid resulting from the first step of simulation has been used as starting liquid in the second step. Even in this case, several attempts (n >100) have been done, crossing various *X-P-T* conditions. The crystallization of ~Fo_{77} olivines from the starting liquid composition can be reproduced only decreasing pressure and temperature at more oxidizing redox conditions and slightly higher water contents. For the second step of simulation, parameters have been therefore set as follows: pressure between 170 and 120 MPa (representative of crystallization at 6-4.5 km of depth for a crust density of 2.8 g/cm^3; cf. Tarasewicz et al., 2012), temperature between 1200-1140°C, fO_2 at the QFM buffer and H_2O = 0.9 wt.% (cf. Keiding and Sigmarsson, 2012). Under these conditions, P3 olivines (~Fo_{77}) starts to crystallize at pressure of 145 MPa, temperature of 1150°C and fO_2 ~1.7×10^{-4} Pa.

The cores of the three olivine populations are flat, i.e., they do not present any compositional zoning over widths of hundreds of μm. This behaviour could reflect residence for significant periods of time at high temperature, allowing complete equilibration through Fe-Mg diffusion prior to the rim overgrowth. Indeed, different zoning features at the rim of the three populations indicate different magmatic histories before the eruption. P1 olivines show peculiar features, as they are namely: a) resorbed with extensive embayments; b) rather scarce (2-3 crystals per thin section); c) typical of the largest phenocrysts (900-2500 μm); d) the most magnesian (Fo_{88}) of the entire dataset; e) with nearly constant core compositions and normally zoned rims (Fig. 4). The core characteristics are typical of unperturbed growth from a melt (hereafter called M1) almost equilibrated with the mantle. The presence of these

crystals suggests that pre-eruptive dynamics have been influenced in some way by the ascent of the M1 magma from the source zones.

P2 olivines (~Fo_{81}) with normal zoning are the most abundant (~70%) in the emitted products. Their crystallization occurred from a magma (hereafter called M2) slightly more evolved than M1. The subordinate reversely zoned envelopes in some P2 olivines (up to ~Fo_{83}) reflect interaction with a magma necessarily more basic, whose olivine crystallizing at equilibrium is more forsteritic than Fo_{83} (Fig. 5). The Fo decrease at the rim of P1 olivines coupled with Fo increase around P2 crystal cores suggest that the mixing process involved M1 and part of M2 in the magma reservoir at the mantle-crust boundary, which is located at ~22 km b.s.l. beneath the Eyjafjallajökull volcano (Tarasewicz et al., 2012 and references therein; Fig. 7). Such deep magma reservoirs are usually present underneath central volcanoes in different areas of Iceland, especially in relation to the most active portions of the rift branches (Searle, 2013 and references therein). Although the precise size of this reservoir beneath Eyjafjallajökull is not known, its bottom and top have been constrained respectively at depths of 24 and 21 km on the grounds of the location of the micro-earthquake foci occurred between March 6 and May 31, 2010 (Tarasewicz et al., 2012; Fig. 7). The result of mixing between M1 and M2 is a hybrid magma (hereafter called M3; Fig. 7), which carried during its ascent the P1 and P2 olivines. We infer that the mixing process within the deep reservoir had very fast timescales because most of the P2 olivines did not register any reverse zoning. This feature could be attributed to lack of complete homogenization of the magma volume involved in the mixing process probably due to the rapid magma ascent towards the surface. This prevented the development of compositional changes in part of the crystals.

Compositional zoning data support the occurrence of a second mixing event at shallower depth. End-members of this second interaction could be M3 and a more evolved magma stored in the crust (hereafter called M4), as suggested by the more fayalitic core compositions

of P3 olivine crystals (~Fo_{77}) with respect to P1 and P2 (Fig. 6). Magma mixing is markedly evident at the rim of P3 olivines, with Fo contents growing from Fo_{77} at the cores to Fo_{82} - Fo_{85} towards the rims (Fig. 6). The presence of the inferred M4 reservoir is supported by InSAR observations, GPS geodetic measurements, and optical tilt leveling data by several authors, who provide evidence of two 4.5 and 6.5 km deep intrusions beneath the Eyjafjallajökull volcano that took place in 1994 and 1999 respectively (Fig. 7; Pedersen and Sigmundsson, 2004; 2006; Sturkell et al. 2003; Sigmundsson et al., 2010). In the next section, time constraints to the above mentioned magma dynamics are provided.

Timescales of magma recharge and transfer

In order to assess timescales of intrusion and open system processes such us magma mixing events before the 2010 Eyjafjallajökull flank eruption, the approach of Costa et al. (2008) and Costa and Morgan (2010) was adopted to model the diffusion-controlled re-equilibration of the Fe-Mg zoning of olivine. In numerical implementations, concentrations are described as a function of space (x) and time (t) and are directly related to values of the diffusion coefficients (D) along the measured profile. Thus, time evolution of the initial concentration distribution of the crystal can be traced until a new profile that fit the observed concentration profile is obtained. Due to the strong diffusion anisotropy, crystals were preliminarily selected to minimize uncertainties on time determination related to the section orientation with respect to the fast diffusion direction (c-axis), following the selection criteria listed in Costa and Chakraborty (2004) and Shea et al. (2015). The modelling has been performed by using Fick's Law-based diffusion equations with concentration dependent diffusion coefficients ($D_{Fe\text{-}Mg}$); we assumed the measured concentration at the rim of the crystals as boundary conditions (see Table ESM 2). The expression for calculating the Fe-Mg diffusion coefficients along [001] is from Dohmen and Chakraborty (2007). Coefficients were

calculated at T = 1210°C, P = 615 MPa and fO_2 at ~3.5×10^{-3} Pa for the P1 and P2 populations, and at T = 1150°C, P = 145 MPa and fO_2 at ~1.7×10^{-4} Pa for the less forsteritic P3 crystals (Table 1). Such parameters have been chosen in accordance with the initial *T*, *P* and fO_2 values of crystallization derived through our MELTS simulations, and are also consistent with the range of crystallization conditions defined for the early basaltic products of the 2010 eruption and the depths of magma storage beneath the volcano as described above (cf. Keiding and Sigmarsson, 2012; Tarasewicz et al., 2012 and references therein). Anisotropy-corrected diffusivity along the direction of the profile (D*trav*) was obtained taking into account how the compositional traverses were oriented with respect to the olivine crystallographic a, b and c axes (respectively coinciding with the optical indicatrix axes X, Y and Z measured by conoscopic observations under a polarizing optical microscope equipped with a Zeiss 4 axis universal stage) to further improve the accuracy and precision on time calculations (cf. Costa and Chakraborty, 2004; Shea et al., 2015). After application of all the correction criteria (i.e. influence of sectioning, diffusion anisotropy, crystal morphology), the model replicates diffusion times with a high degree of precision, although the number crystals suitable for calculation is considerably reduced (Table 1; ESM 2). Uncertainties are mainly related to the temperature and oxygen fugacity determination. A temperature uncertainty of ±10°C yields errors of 1 day (2σ) on the timescale estimates; fO_2 variation of one order magnitude produces errors of ca. 3 days (2σ). Conversely, the pressure dependence is small, with time oscillations of ca. 1 hour for pressure changes of 10 MPa, at constant temperature and fO_2.

The chemical records preserved in olivine cores of the basalts erupted at Fimmvörðuháls Pass are evidence of at least three compositionally distinct magmatic environments where crystals grew close to equilibrium. Later, at the rims, they developed chemical gradients as a consequence of changed conditions. Awareness of the magmatic process causing

374 disequilibrium in olivines is important to set the initial composition before re-equilibration of
375 the system through diffusion. The high and constant Fo content at the P1 crystal core implies
376 an early growth stage in a primitive host magma under unperturbed chemical and physical
377 conditions. The decreased Fo content at the rims of the P1 crystals has been attributed to
378 interactions with more evolved magmas during the intrusion at crustal levels, in order to
379 achieve the new chemical and physical equilibrium at lower Fo. Therefore, through the Fe-
380 Mg diffusion model we tried to estimate the timescale of this early intrusion and mixing at
381 crustal depth (Fig. 4). The presence of at least two magma storage zones beneath
382 Eyjafjallajökull volcano has been recognized through the zoning patterns preserved in the P2
383 and P3 olivine crystals (Figs. 5 and 6). Indeed, the core compositions at Fo_{81} (P2) and Fo_{77}
384 (P3) suggest their growth in different magma environments, from melts more evolved than
385 that of the P1 crystals. Reverse Fo zoning at the rim of both populations reflects mixing
386 consequent to mafic recharge. These two recharging events produced chemical gradients at
387 the crystal rims, and are considered responsible for triggering diffusion. Modelling of the
388 chemical zoning in P2 and P3 olivines leads then to define timing of these mixing events
389 (Figs. 5 and 6).

390 Based on our calculations, the chemical zoning of P1 crystals requires ~34 days to re-
391 equilibrate through diffusion; this result matches well the timescale obtained for the diffusion
392 event in P2 crystals (30 days on average), suggesting an interaction between the P1 and P2
393 host magmas about one month before the emission of the analysed products on April 10-12
394 (Figs. 4 and 5; Table1). The micro-earthquake locations provided by Tarasewicz et al. (2012)
395 confirm that a magma intrusion occurred at 21-24 km of depth about one month before the
396 2010 flank eruption at Eyjafjallajökull (Fig. 7). The more evolved P3 olivines record
397 timescales of re-equilibration that are significantly shorter than those obtained for P1 and P2
398 crystals (Fig. 6). Time estimations indicate that the second mixing event recorded by rims of

399 the P3 olivines occurred about two weeks before magma emission at the Fimmvörðuháls Pass
400 (see Table1). Even in this case, micro-earthquake locations corroborate the assumption that
401 the second event of interaction took place between 6.5 and 4.5 km of depth and that this final
402 event of magma mixing was the triggering mechanism for the intrusion of an E-W-oriented
403 dyke from the shallow storage zone up to the Fimmvörðuháls Pass (Fig. 7; cf. Tarasewicz et
404 al., 2012).

405 Considering that the distance covered by the intruding magma between the sites of the two
406 mixing processes is ~17 km and that the obtained timescales for the two mixing events are
407 ~30 and ~15 days respectively, the calculated average magma ascent rate is in the order of
408 0.01 m/sec. These ascent rates refer to magma migration in the deep levels of the
409 Eyjafjallajökull plumbing system, and are well in the range expected for basaltic liquids (e.g.,
410 Rutherford, 2008, and references therein; Armienti et al., 2013). Evaluation of the ascent rate
411 at shallow levels is more complex due to the influence of several variables (i.e., gas
412 exsolution, conduit dynamics, fracture opening etc.). In this regard, literature data for other
413 basaltic volcanoes indicate extrusive ascent rates, especially for the early explosive phase of
414 the eruption, up to one order of magnitude higher than those derived for migration in the deep
415 levels of the plumbing system (cf. Rutherford, 2008, and references therein).

416

417 **Implications**

418 The Fe-Mg diffusion modelling in olivine chemical profiles found in products of the 2010
419 eruption at the Fimmvörðuháls Pass (Eyjafjallajökull volcano, Iceland) have been used to
420 reconstruct the pre-eruptive history of the emitted magmas. Our approach has led to the
421 comprehension of the dynamics of magmatic processes and of their timescales prior to the
422 eruption. All the data available support the idea of a multi-level storage system beneath the
423 Eyjafjallajökull volcano, where a poorly evolved magma ascending to the surface experienced

multiple events of mixing with other magmas slightly different in their evolutionary degree. The equilibration through diffusion in three olivine populations, as a consequence of the interactions, constrains the timescales of transfer dynamics from the deep levels of the plumbing system (21-24 km of depth) towards the shallow reservoirs (4.5-6.5 km of depth) at ascent rates estimated at 0.01 m/sec. Our study elucidates the physical configuration of volcanic systems grown in ocean ridge settings, emphasizing the possibility that magmas undergo complex processes during their storage and transport in the crust. Since the evidence of the first intrusion, the magma upraises from deep levels of the feeding system to the surface in a short timespan; this means that injection of primitive magmas in the deep reservoirs can trigger significant eruptions in rather short times.

Acknowledgements

Field-work and the analytical results presented in this study have been made possible through financial support from the University of Catania (Italy) to Marco Viccaro. Comments, suggestions and corrections provided by the Associate Editor G. Zellmer, and the reviewers Corliss K.I. Sio and Christy B. Till helped to improve quality and clarity of this paper.

References cited

Armienti, P., Perinelli, C., and Putirka, K.D. (2013) A New Model to Estimate Deep-level Magma Ascent Rates, with Applications to Mt. Etna (Sicily, Italy). Journal of Petrology, 54, 795-813.

Costa, F., Chakraborty, S., and Dohmen, R. (2003) Diffusion coupling between trace and major elements and a model for calculation of magma residence times using plagioclase. Geochimica et Cosmochimica Acta, 67, 2189-2200.

448 Costa, F., Dohmen, R., and Chakraborty, S., (2008) Timescales of magmatic processes from
449 modeling the zoning patterns of crystals. In: Putirka, K.D., Tepley III, F., J., (eds)
450 Minerals, Inclusions and Volcanic Processes. Reviews in Mineralogy and
451 Geochemistry 69, Mineralogical Society of America, Chantilly, VA, USA, 545-594.
452 Costa, F., and Chakraborty, S., (2004) Decadal time gap between mafic intrusion and silicic
453 eruption obtained from chemical zoning patterns in olivine. Earth and Planetary
454 Science Letters, 227, 517-530.
455 Costa, F., and Morgan, D. J. (2010) Time constraints from chemical equilibration in
456 magmatic crystals. In: Dosseto, A., Turner, S.P., Van Orman, J.A. (eds) Timescales of
457 magmatic processes: from core to atmosphere. Wiley-Blackwell, West Sussex, 125-
458 159.
459 Dohmen, R., and Chakraborty, S. (2007b) Fe-Mg diffusion in olivine II: point defect
460 chemistry, change of diffusion mechanisms and a model for calculation of diffusion
461 coefficients in natural olivine. Physics and Chemistry of Minerals, 34, 597-598.
462 Dugmore, A.J., Newton, A. J., Smith, K.T., and Mairs, K.A. (2013) Tephrochronology and
463 the late Holocene volcanic and flood history of Eyjafjallajökull, Iceland. Journal of
464 Quaternary Science, 28, 237-247.
465 Dunn, R.A., Toomey, D.R., and Solomon, S.C. (2000) Three-dimensional seismic structure
466 and physical properties of the crust and shallow mantle beneath the East Pacific Rise
467 at 9 degrees 30'N. Journal of Geophysical Research - Solid Earth, 105, B10, 23537-
468 23555.
469 Ginibre, C., Woerner, G., and Kronz, A. (2007) Crystal zoning as an archive for magma
470 evolution. Elements, 3, 261-266.
471 Gudmundsson, M.T., Pedersen, R., Vogfjörd, K., Thorbjarnardóttir, B., Jakobsdóttir, S., and
472 Roberts, M.J. (2010) Eruptions of Eyjafjallajökull Volcano, Iceland. Eos, 91, p. 191;

Herzberg, C., and O'Hara, M.J. (1998) Phase equilibrium constraints on the origin of basalts, picrites, and komatiites. Earth Science – Reviews, 44, 39-79.

Kahl, M., Chakraborty, S., Costa, F., and Pompilio, M. (2011) Dynamic plumbing system beneath volcanoes revealed by kinetic modeling and the connection to monitoring data: an example from Mt. Etna. Earth and Planetary Science Letters, 308, 11-22.

Kahl, M., Chakraborty, S., Costa, F., Pompilio, M., Liuzzo, M., and Viccaro, M. (2013) Compositionally zoned crystals and real-time degassing data reveal changes in magma transfer dynamics during the 2006 summit eruptive episodes of Mt. Etna. Bulletin of Volcanology, 75, 692.

Keiding, J.K., and Sigmarsson, O. (2012) Geothermobarometry of the 2010 Eyjafjallajökull eruption: New constraints on Icelandic magma plumbing systems. Journal of Geophysical Research - Solid Earth, 117, B00C09.

Morgan, D.J., Blake, S., Rogers, N.W., De Vivo, B., Rolandi, G., Macdonald, R., and Hawkesworth, C.J. (2004) Time scales of crystal residence and magma chamber volume from modelling of diffusion profiles in phenocrysts: Vesuvius 1944. Earth and Planetary Science Letters, 222, 933-946.

Morgan, D.J., and Blake, S. (2006) Magmatic residence times of zoned phenocrysts: introduction and application of the binary element diffusion modelling (BEDM) technique. Contribution to Mineralogy and Petrology, 151, 58-70.

Moune, S., Sigmarsson, O., Schiano, P., Thordarson, T., and Keiding, J.K. (2012) Melt inclusion constraints on the magma source of Eyjafjallajökull 2010 flank eruption. Journal of Geophysical Research - Solid Earth, 117, B00C07.

Pedersen, R., and Sigmundsson, F. (2004) InSAR based sill model links spatially offset areas of deformation and seismicity for the 1994 unrest episode at Eyjafjallajökull volcano, Iceland. Geophysical Research Letters, 31, L14610.

Pedersen, R., and Sigmundsson, F. (2006) Temporal development of the 1999 intrusive episode in the Eyjafjallajökull volcano, Iceland, derived from InSAR images. Bulletin of Volcanology, 68, 377-393.

Putirka, K.D. (2005) Igneous thermometers and barometers based on plagioclase plus liquid equilibria: Tests of some existing models and new calibrations. American Mineralogist, 99, 336-346.

Roeder, P.L., and Emslie, R.F. (1970) Olivine-liquid equilibrium. Contribution to Mineralogy and Petrology, 29, 275-289.

Rutherford, M.J. (2008) Magma Ascent Rates. In: Putirka, K.D., Tepley III, F., J., (eds) Minerals, Inclusions and Volcanic Processes. Reviews in Mineralogy and Geochemistry 69, Mineralogical Society of America, Chantilly, VA, USA, 241-271.

Searle, R. (2013) Mid-Ocean Ridges. Cambridge University Press, 330 pp.

Shea, T., Costa, F., Krimer, D., and Hammer, J.E. (2015) Accuracy of timescales retrieved from diffusion modeling in olivine: a 3D perspective. American Mineralogist, in press, doi:10.2138/am-2015-5163.

Sigmundsson, F., Hreinsdottir, S., Hooper, A., Arnadottir, T., Pedersen, R., Roberts, M. J., Oskarsson, N., Auriac, A., Decriem, J., Einarsson, P., Geirsson, H., Hensch, M., Ofeigsson, B.G., Sturkell, E., Sveinbjornsson, H., and Feigl, K.L. (2010) Intrusion triggering of the 2010 Eyjafjallajökull explosive eruption. Nature, 468, 426-U253.

Sigmarsson, O., Vlastelic, I., Andreasen, R., Bindeman, I., Devidal, J. L., Moune, S., Keiding, J. K., Larsen, G., Hoskuldsson, A., and Thordarson, T. (2011) Remobilization of silicic intrusion by mafic magmas during the 2010 Eyjafjallajökull eruption. Solid Earth, 2, 271-281.

Streck, M. J. (2008) Mineral Textures and Zoning as Evidence for Open System Processes. In: Putirka, K.D., Tepley III, F., J., (eds) Minerals, Inclusions and Volcanic Processes.

Reviews in Mineralogy and Geochemistry 69, Mineralogical Society of America, Chantilly, VA, USA, 595-622.

Sturkell, E., Sigmundsson, F., and Einarsson, P. (2003) Recent unrest and magma movements at Eyjafjallajökull and Katla volcanoes, Iceland. Journal of Geophysical Research - Solid Earth, 108, B8, 2369.

Tarasewicz, J., Brandsdottir, B., White, R. S., Hensch, M., and Bergthora, T. (2012) Using microearthquakes to track repeated magma intrusions beneath the Eyjafjallajökull stratovolcano, Iceland. Journal of Geophysical Research - Solid Earth, 117, B00C06.

Thordarson, T., and Larsen, G. (2007) Volcanism in Iceland in historical time: Volcano types, eruption styles and eruptive history. Conference: Penrose Conference on Beyond the Plume Hypothesis, Tests of the Plume Paradigm and Alternatives Location: Hverageroi, Iceland, AUG 25-29, 2003. Journal of Geodynamics, 43, 118-152.

Toplis, M.J. (2005) The thermodynamics of iron and magnesium partitioning between olivine and liquid: criteria for assessing and predicting equilibrium in natural and experimental systems. Contribution to Mineralogy and Petrology, 149, 22-39.

Viccaro, M., Giacomoni, P.P., Ferlito, C., and Cristofolini, R. (2010) Dynamics of magma supply at Mt. Etna volcano (Southern Italy) as revealed by textural and compositional features of plagioclase phenocrysts. Lithos 116, 77-91.

Wallace, G.S., and Bergantz, G.W. (2002) Wavelet-based correlation (WBC) of zoned crystal populations and magma mixing. Earth and Planetary Science Letters, 202, 133-145.

Wallace, G.S., and Bergantz, G.W. (2004) Constraints on mingling of crystal populations from off-center zoning profiles: A statistical approach. American Mineralogist, 89, 64-73.

Wallace, G.S., and Bergantz, G.W. (2005) Reconciling heterogeneity in crystal zoning data: An application of shared characteristic diagrams at Chaos Crags, Lassen Volcanic Center, California. Contribution to Mineralogy and Petrology, 149, 98-112.

Zellmer, J. F., Blake, S., Vance, D., Hawkesworth, C., and Turner, S. (1999) Plagioclase residence times at two island arc volcanoes (Kameni Islands, Santorini, and Soufriere, St. Vincent) determined by Sr diffusion systematics. Contribution to Mineralogy and Petrology, 136, 345-357.

List of figure captions

Figure 1 – a) Schematic map of Iceland with composition of the volcanic rocks belonging to different neo-volcanic zones. b) Digital Elevation Model of the Eyjafjallajökull and Katla volcanoes and the area of Fimmvörðuháls Pass (source www.lmi.is/en/okeypis-kort/).

Figure 2 – A and B) Scoria cones and a'a lava flow field at Fimmvörðuháls Pass; C) Part of the lava flow field at the Fimmvörðuháls Pass with top of the Eyjafjallajökull volcano on the background; D) Lava flow field at the Fimmvörðuháls Pass with the Myrdalsjökull glacier on the background.

Figure 3 – a) Photo taken under the polarized light microscope (crossed Nicols) showing the petrographic features of a representative basalt emitted during the 2010 eruption at the Fimmvörðuháls Pass; b) c) d) BSE images taken at the scanning electron microscope of representative P1, P2 and P3 olivine crystals respectively.

Figure 4 – X-ray map for Mg, rim-to-rim zoning profile (white line on the X-ray map) and Fe-Mg diffusion modelling for a representative P1 olivine crystal, with ~Fo_{88} core and normal

571 zoning at the rim, found in the basalts emitted at the Fimmvörðuháls Pass during the 2010
572 eruption. The figure shows the rim-to-rim profile for the forsterite concentration (Fo%)
573 measured on the E8_Ol5 olivine (circles). The black dashed line indicates the initial
574 concentration profile prior to the diffusion, whereas the red line reveals the best-fit
575 diffusion model for the observed zoning profile. The stereographic plot indicates the
576 angular relations between the a, b and c crystallographic axes in olivine and the directions
577 of the measured rim-to-rim traverse.
578
579 Figure 5 – X-ray map for Mg, rim-to-rim zoning profile (white line on the X-ray map) and Fe-
580 Mg diffusion modelling for a representative P2 olivine crystal, with ~Fo_{81} core and reverse
581 zoning at the rim, found in the basalts emitted at the Fimmvörðuháls Pass during the 2010
582 eruption. The figure shows the rim-to-rim profile for the forsterite concentration (Fo%)
583 measured on the E8_Ol1 olivine (circles). The black dashed line indicates the initial
584 concentration profile prior to the diffusion, whereas the red line reveals the best-fit
585 diffusion model for the observed zoning profile. The stereographic plot indicates the
586 angular relations between the a, b and c crystallographic axes in olivine and the directions
587 of the measured rim-to-rim traverse.
588
589 Figure 6 – X-ray map for Mg, rim-to-rim zoning profile (white line on the X-ray map) and Fe-
590 Mg diffusion modelling for a representative P1 olivine crystal, with ~Fo_{77} core and marked
591 reverse zoning at the rim, found in the basalts emitted at the Fimmvörðuháls Pass during
592 the 2010 eruption. The figure shows the rim-to-rim profile for the forsterite concentration
593 (Fo%) measured on the E15_Ol5 olivine (circles). The black dashed line indicates the
594 initial concentration profile prior to the diffusion, whereas the red line reveals the best-fit
595 diffusion model for the observed zoning profile. The stereographic plot indicates the

596 angular relations between the a, b and c crystallographic axes in olivine and the directions
597 of the measured rim-to-rim traverse.
598
599 Figure 7 – Cartoon of the petrological evolution leading to the 2010 eruption at the
600 Fimmvörðuháls Pass and at the summit of Eyjafjallajökull volcano. Moho discontinuity is
601 reported at ca. 22 km b.s.l. (cf. Tarasewicz et al., 2012 and references therein). Blue dots
602 represent the locations of earthquake hypocentres during the period March 6 - May 31,
603 2010. The magmatic history starts with ascent from the mantle of the primitive magma
604 (M1) carrying P1 olivines (with Fo_{88} cores). Considering that the analysed products have
605 been erupted between April 10 and 12, 2010, the diffusion modelling of P1 olivines dates a
606 first event of intrusion of M1 into a deep magma environment ~34 days before the
607 emission that coincide with the first detected earthquakes at 23-26 km of depth. At this
608 depth, M1 magma mixed with the residing slightly more evolved magma (M2) that bears
609 P2 olivines (with Fo_{81} cores). Mixing between M1 and M2 produced a new magma (M3),
610 as testified by reverse Fo zoning (up to Fo_{83}) in some P2 crystals. Diffusion modelling
611 dates this mixing event between 28 and 33 days before the emission on April 10-12, 2010.
612 M3 magma started its ascent carrying P1 and P2 olivines and mixed at 4.5-6 km b.s.l. with
613 a residing magma (M4) already intruded during 1994 and 1999 (Pedersen and
614 Sigmundsson, 2004; 2006; Sturkell et al. 2003; Sigmundsson et al., 2010) that bears P3
615 olivines (with Fo_{77} cores). This mixing event, testified by reverse Fo zoning (Fo_{82-85}) in P3
616 olivines, is dated by diffusion modelling between 12 and 18 days before the emission of
617 the April 10-12 lavas. Result of this second mixing event is the final hybrid magma that
618 intruded through an E-W-oriented dyke and was erupted at the Fimmvörðuháls Pass (M5)
619 between March 20 and April 12, 2010. The trachyandesitic magma reservoir that mixed

620 with less differentiated magma on April 12 (Sigmarsson et al., 2011) is reported in the
621 figure.

A

Kolbeinsey

Kolbeinsey Ridge

Krafla

North Volcanic Zone

Askja

Snæfellness Zone

West Volcanic Zone

Laki-Fogrufjoll

Grímsvötn

Öræfajökull Belt

East Volcanic Zone

Hekla

Vatnafjöll

Reykjanes Ridge

Eyjafjallajökull

Surtsey

Heimaey

Katla

The Westman Islands

Atlantic Ocean

Main volcanoes

Tholeiitic basalt

Alkalic basalt

Transitional alkali basalt

Late Pleistocene/ Holocene rocks

Other rocks

Ice caps

B

Katla

Eyjafjallajökull

Fimmvörðuháls Pass

0 5 10 15 20

Km

Figure 2

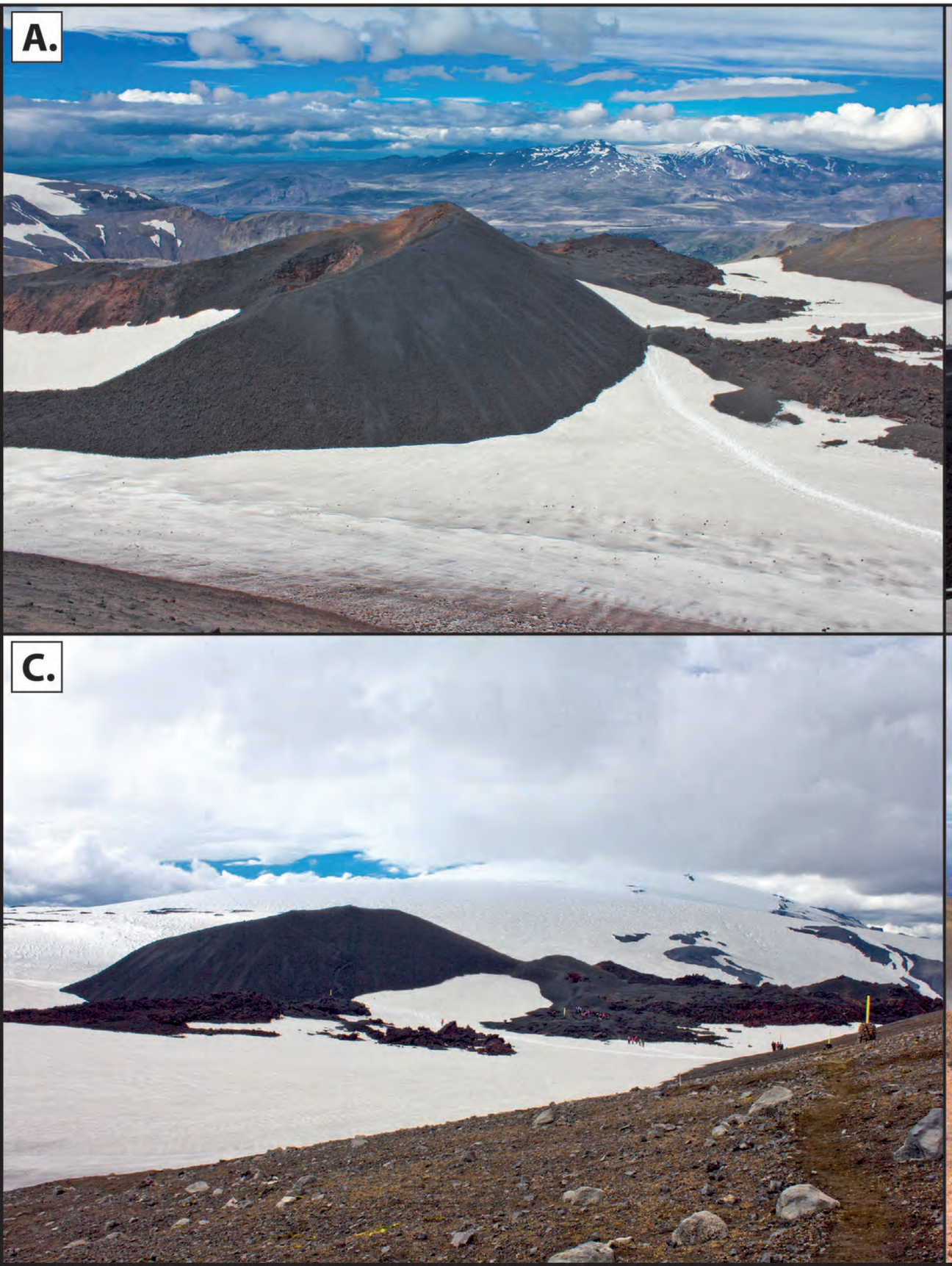

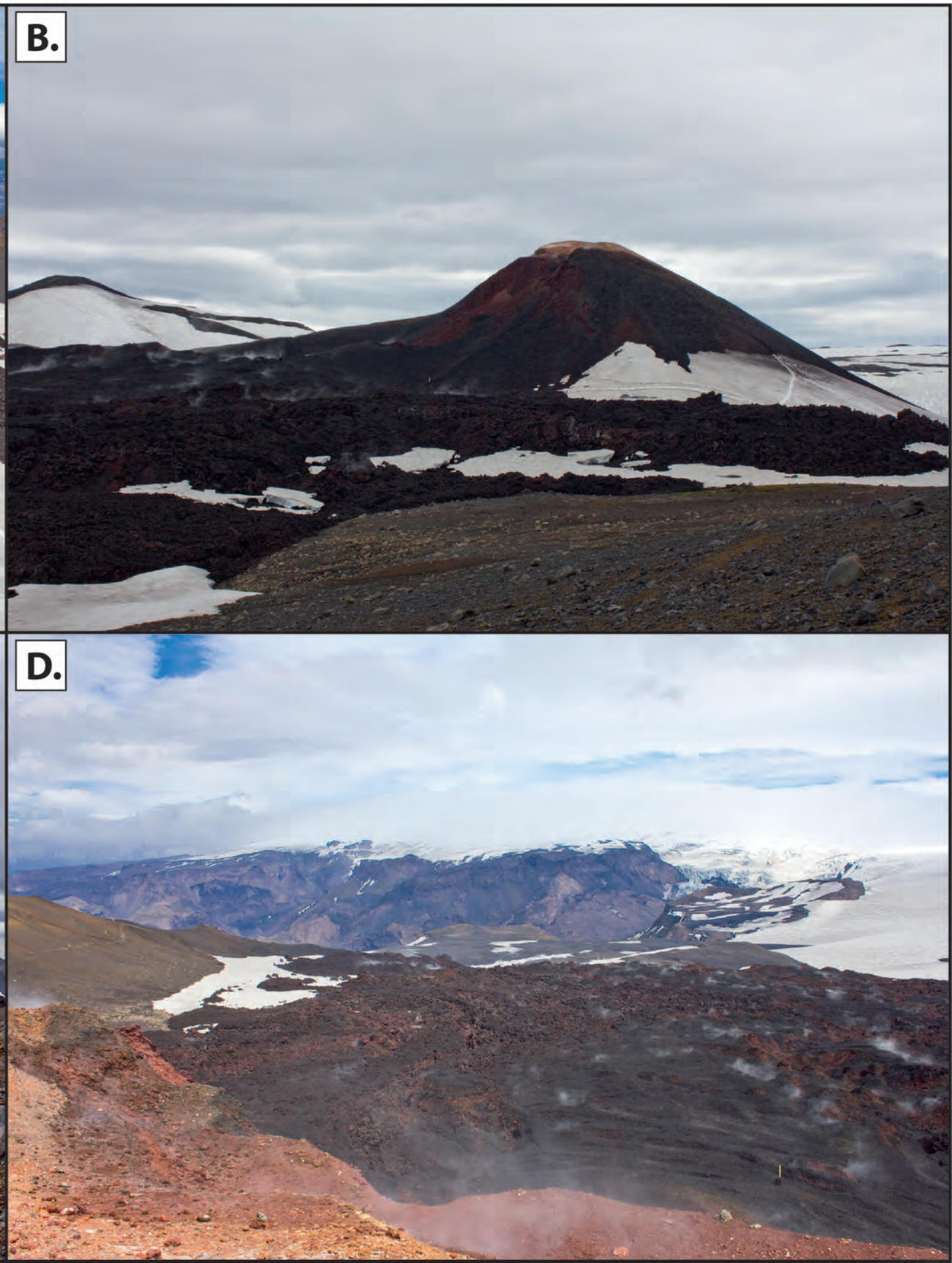

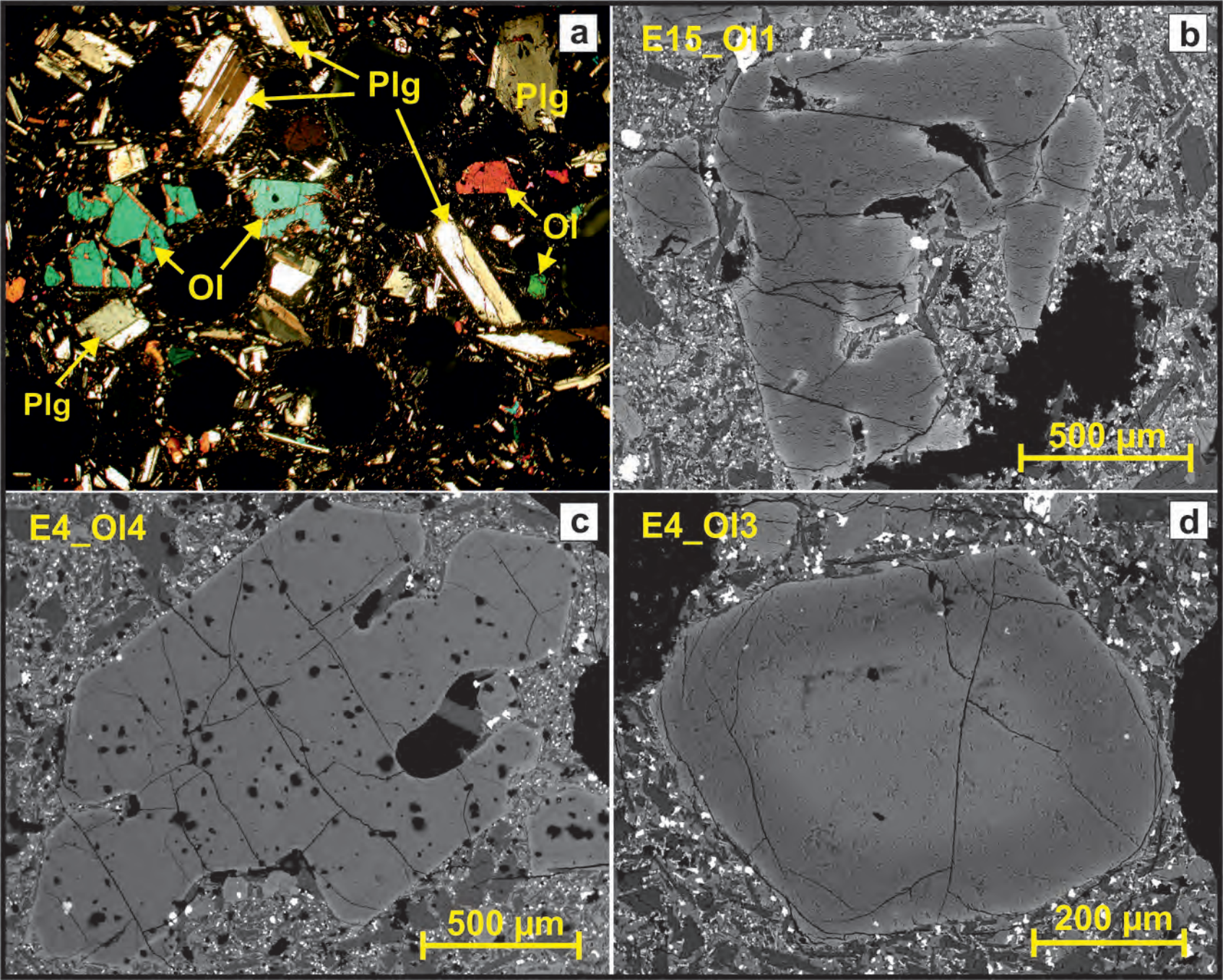
a
Plg
Plg
Ol
Ol
Plg
b
E15_Ol1
500 µm
c
E4_Ol4
500 µm
d
E4_Ol3
200 µm

Figure 3

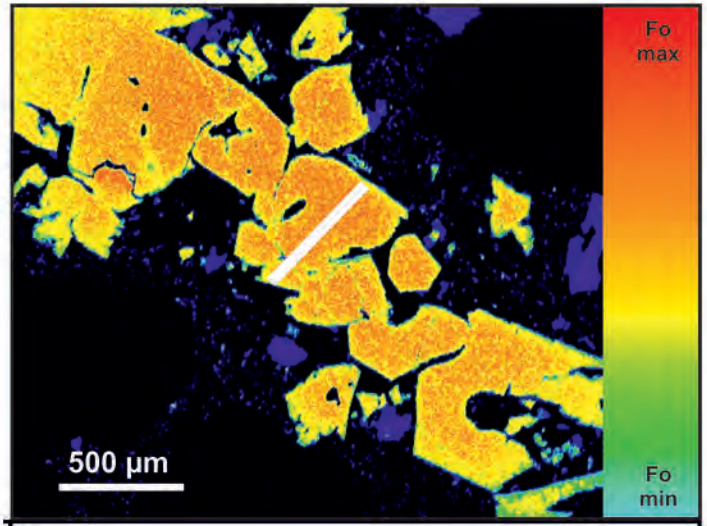

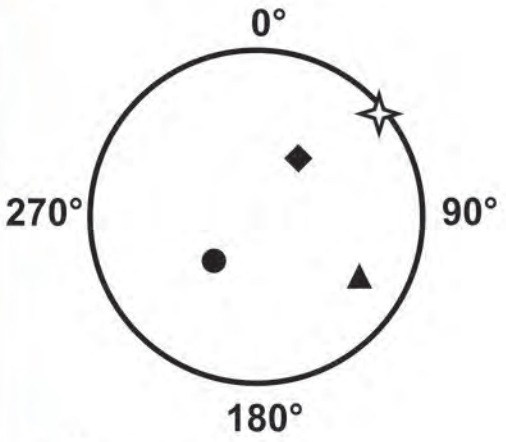

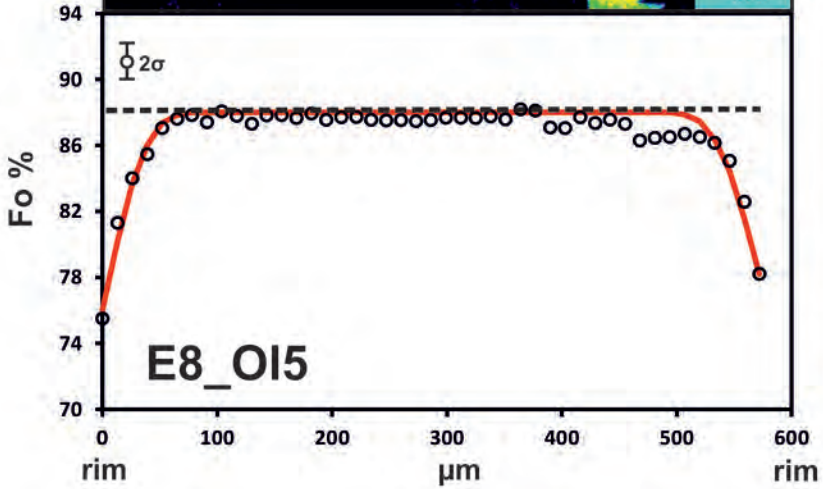

Measured profile

Initial profile

Best-fit diffusion curve

Figure 4

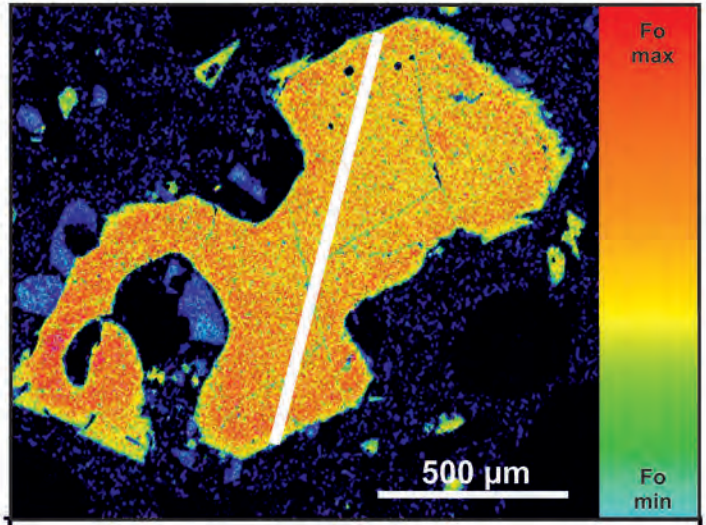

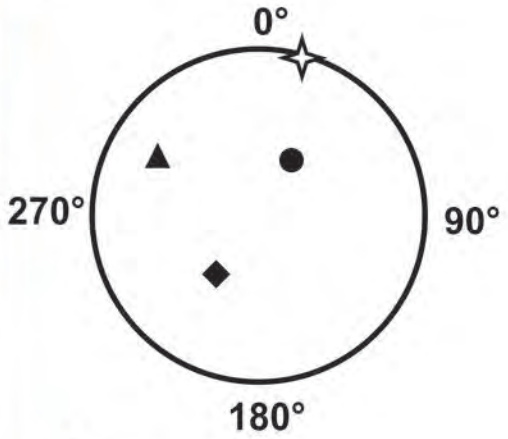

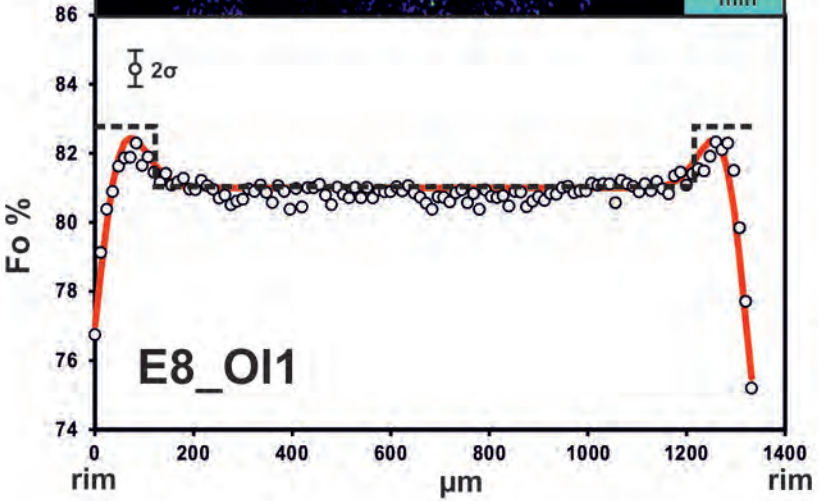

Measured profile

Initial profile

Best-fit diffusion curve

Figure 5

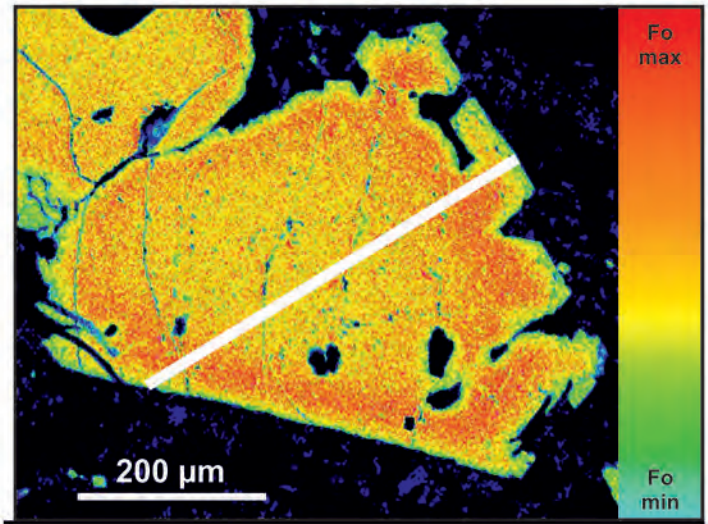
Fo max
Fo min
200 µm

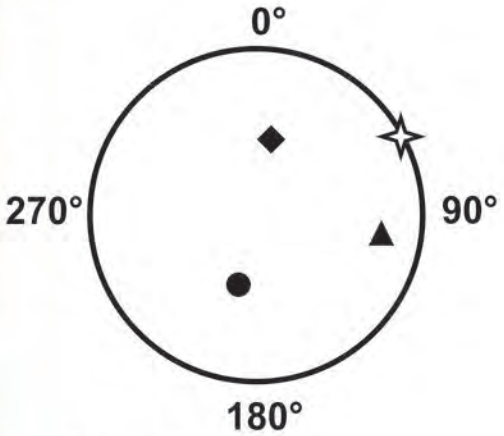
0°
90°
180°
270°
profile
a-axis
b-axis
c-axis

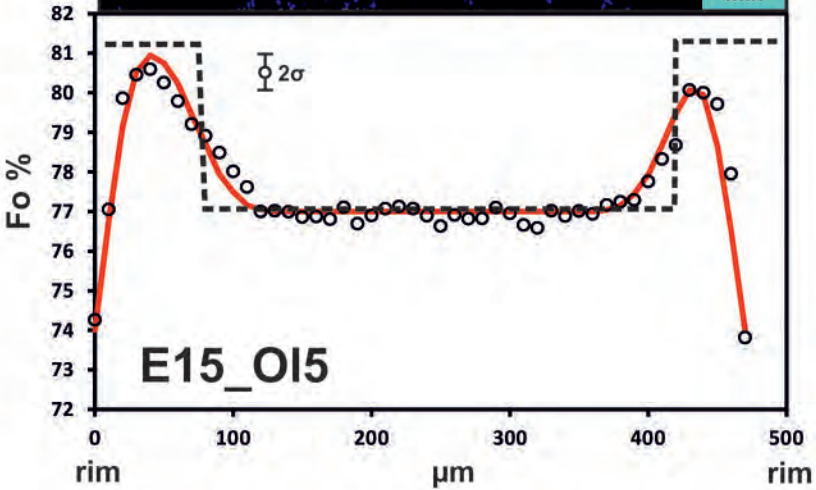
Fo %
2σ
E15_Ol5
rim
µm
rim
Measured profile
Initial profile
Best-fit diffusion curve

Figure 6

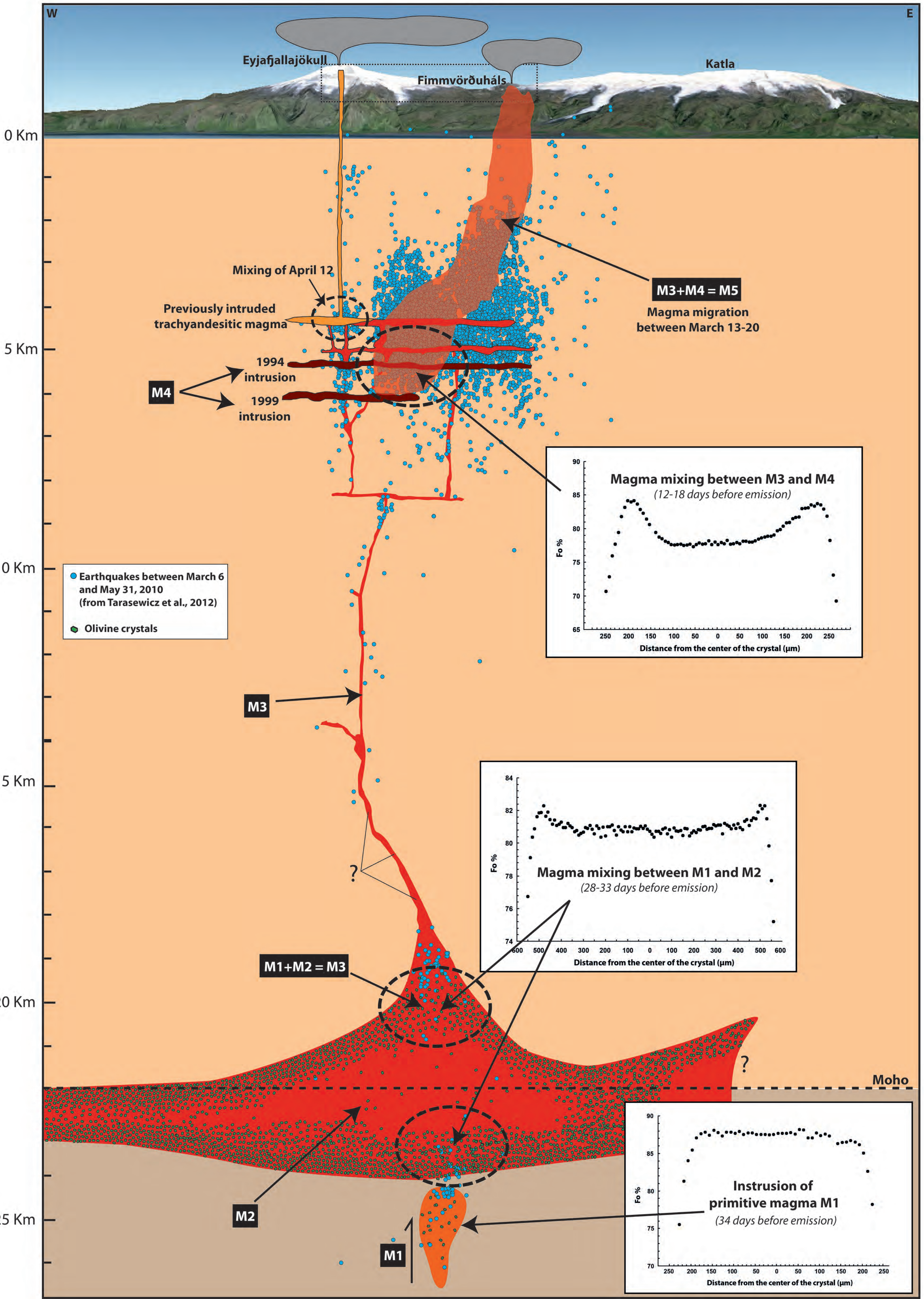
W
E
Eyjafjallajökull
Fimmvörðuháls
Katla
0 Km
5 Km
10 Km
15 Km
20 Km
25 Km
Mixing of April 12
Previously intruded trachyandesitic magma
1994 intrusion
1999 intrusion
M4
M3
M1+M2 = M3
M2
M1
M3+M4 = M5
Magma migration between March 13-20
Earthquakes between March 6 and May 31, 2010 (from Tarasewicz et al., 2012)
Olivine crystals
Moho
?
?
Magma mixing between M3 and M4
(12-18 days before emission)
Fo %
Distance from the center of the crystal (µm)
Magma mixing between M1 and M2
(28-33 days before emission)
Fo %
Distance from the center of the crystal (µm)
Instrusion of primitive magma M1
(34 days before emission)
Fo %
Distance from the center of the crystal (µm)

Table 1 - Calculated timescales of re-equilibration and main parameters used for modeling the Fe-Mg diffusion of selected olivine crystals from the 2010 basaltic eruption at Eyjafjallajökull.

Population	Olivine	Core composition (Fo %)	Temperature (°C)	Pressure (Kbars)	fO_2 (Pa)	Dtrav ($\mu m^2 * s^{-1}$)	Average Time (days)
P1	E8_Ol5	88	1210	6.15	$3.55*10^{-4}$	$1.31*10^{-4}$	34
P2	E4_Ol2	81	1210	6.15	$3.55*10^{-5}$	$4.61*10^{-4}$	33
P2	E8_Ol1	81	1210	6.15	$3.55*10^{-5}$	$2.94*10^{-4}$	28
P3	E4_Ol5	77	1150	1.45	$2.19*10^{-5}$	$1.05*10^{-4}$	18
P3	E15_Ol5	77	1150	1.45	$2.19*10^{-5}$	$1.63*10^{-4}$	18
P3	E15_Ol7	77	1150	1.45	$2.19*10^{-5}$	$2.95*10^{-4}$	12
P3	E3_Ol1	78	1150	1.45	$2.19*10^{-5}$	$2.35*10^{-4}$	18
P3	E15_Ol6	78	1150	1.45	$2.19*10^{-5}$	$1.00*10^{-4}$	16
P3	E8_Ol4	79	1150	1.45	$2.19*10^{-5}$	$1.05*10^{-4}$	12